Nat. Struct. Mol. Biol. **20**, 502–507 (2013)

Macrodomain-containing proteins are new mono-ADP-ribosylhydrolases

Florian Rosenthal, Karla L H Feijs, Emilie Frugier, Mario Bonalli, Alexandra H Forst, Ralph Imhof, Hans C Winkler, David Fischer, Amedeo Caflisch, Paul O Hassa, Bernhard Lüscher & Michael O Hottiger

In the version of this supplementary file originally posted online, Ile189 was incorrectly referred to as Ile89 in **Supplementary Figure 4e**. The error has been corrected in this file as of 3 April 2013.

Supplementary material for:

Macrodomain-containing proteins are novel mono-ADP-ribosylhydrolases

Florian Rosenthal, Karla L.H. Feijs, Emilie Frugier, Mario Bonalli, Alexandra H. Forst, Ralph Imhof, Hans C. Winkler, David Fischer, Amedeo Caflisch, Paul O.Hassa, Bernhard Lüscher and Michael O. Hottiger

Supplementary Figure 1

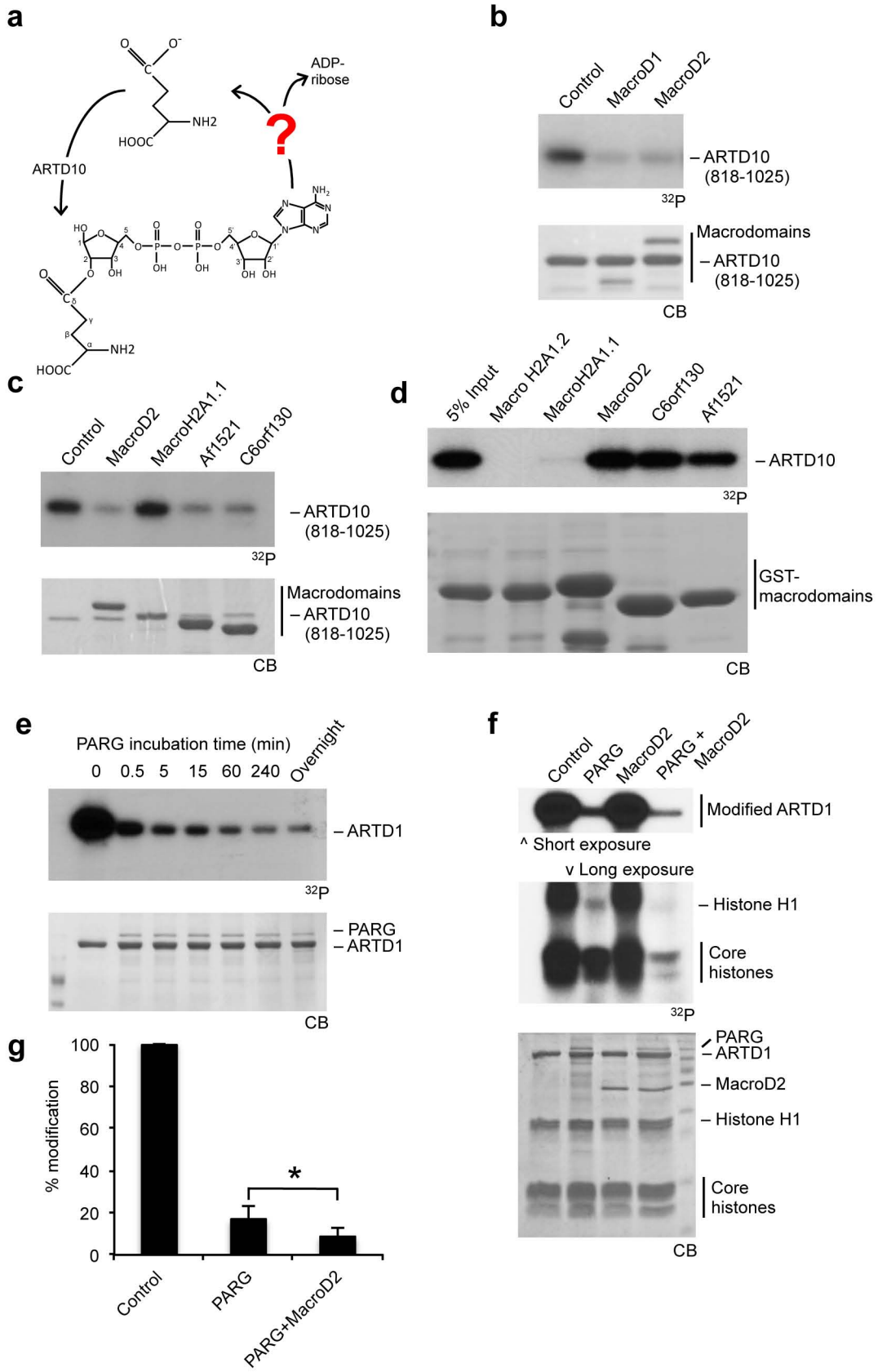

Supplementary Figure 1. Macrodomain-containing proteins hydrolyze mono-ADP-ribose modifications. (a) The missing link in the protein mono-ADP-ribosylglutamate modification cycle. (b-c) MacroD1, MacroD2, Af1521 and C6orf130 hydrolyze mono-ADP-ribosylated catalytic ARTD10 domain (residues 818-1025), while MacroH2A1.1 did not show activity. (d) ADP-ribose binding to different macrodomain proteins. Tagged macrodomain proteins were immobilized and incubated with automodified ARTD10. (e) Protein poly-ADP-ribose hydrolyzing activity of PARG. ARTD1 was auto-ADP-ribosylated *in vitro* with radioactive NAD^+ and subjected to de-ADP-ribosylation assays with recombinant PARG for the indicated times. (f) PARG treatment renders proteins modified by ARTD1 under low NAD^+ concentrations partly susceptible to hydrolysis by MacroD2. (g) MacroD2 further demodifies PARG treated ARTD1. ARTD1 was auto-poly-ADP-ribosylated and consecutively demodified either by PARG alone or by PARG and MacroD2. Three independent experiments were quantified and the results are shown relative to the untreated control (mean ± SD). The effect of MacroD2 treatment on PARG treated samples was significant based on a paired t-test ($p < 0.05$).

Supplementary Figure 2

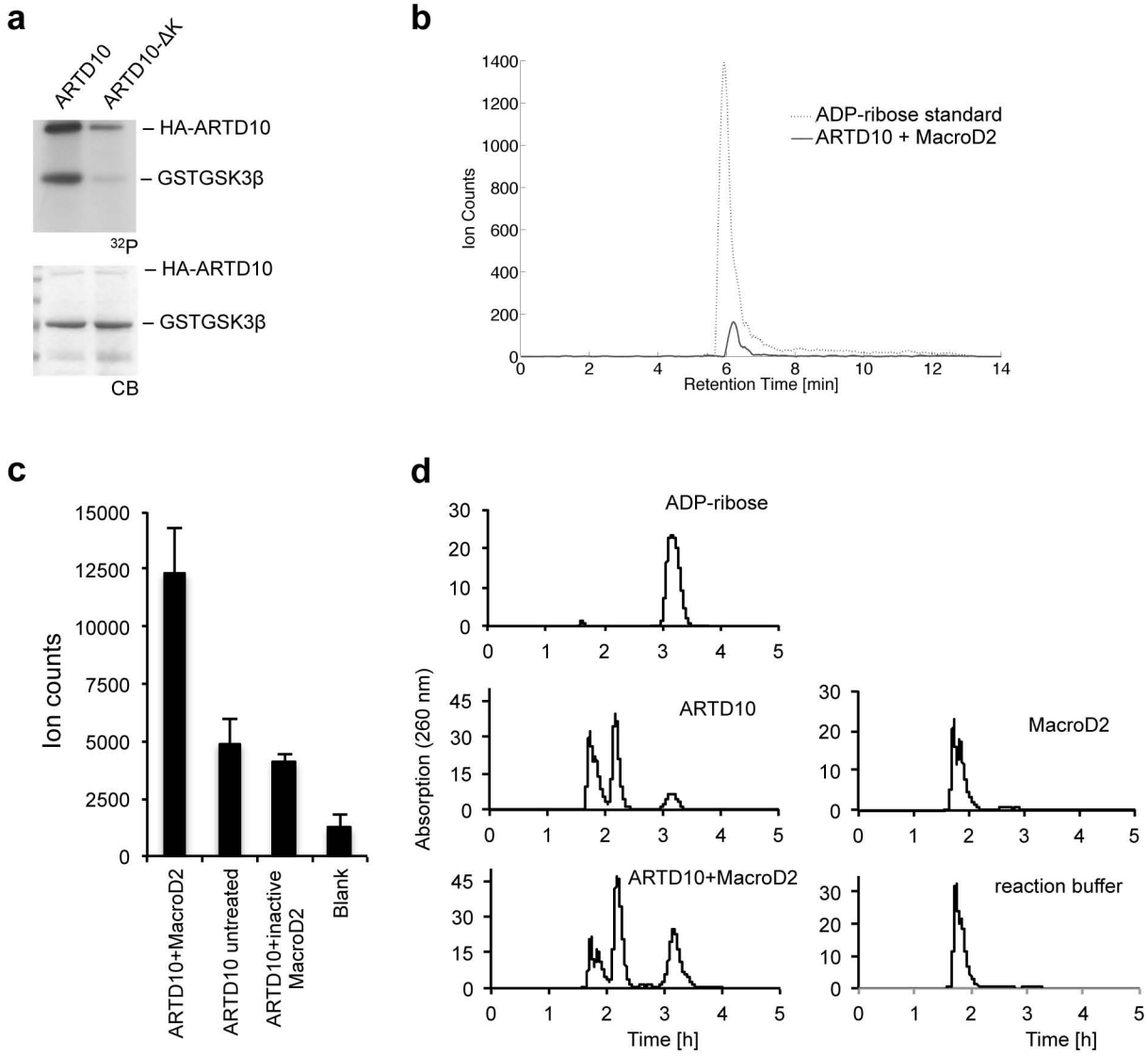

Supplementary Figure 2. Identification of ADP-ribose as the product released by MacroD2 from auto-modified ARTD10. (a) The ARTD10-ΔK mutant shows reduced ADP-ribosylation activity toward itself and GSK3β. (b) Extracted ion chromatograms of 558.064, monoisotopic mass of released ADP-ribose and ADP-ribose standard [M-H] adduct. Elution time window of ADP-Ribose can be observed between 6 and 7 minutes. (c) Relative amounts of ADP-ribose. MS scans in the elution time range of ADP-ribose were combined and the ion abundance of mass 558.064 is displayed. Error bars: standard deviation of three replicate LC-MS runs. (d) MacroD2 releases ADP-ribose from mono-ADP-ribosylated ARTD10 substrate. Reactions products were separated by HPLC on a RP C18 column and detected by measuring absorption at 260 nm.

Supplementary Figure 3

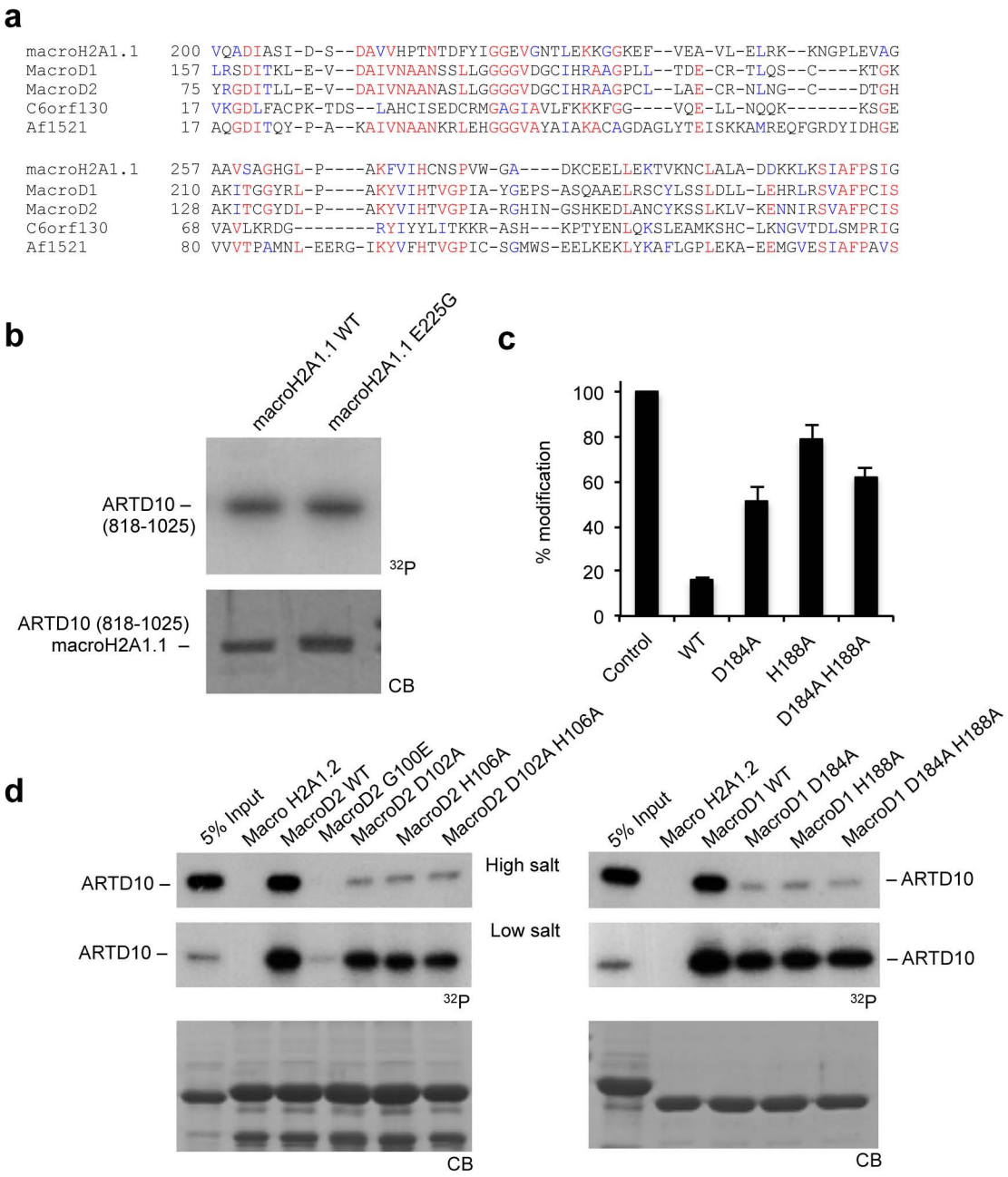

Supplementary Figure 3. Identification of residues implicated in catalysis.

(a) Sequence alignment of macrodomain containing proteins from *Homo sapiens* (macroH2A 1.1, MacroD1, MacroD2, C6orf130), and *Archaeoglobolus fulgidus* (Af1521). Only the amino acids aligning to the residues 157 - 286 of the MacroD1 macrodomain are shown. (b) Mutation of E225 of macroH2A1.1 to a glycine does not restore mono-ADP-ribose hydrolyzing activity. (c) Mutational analysis of MacroD1 highlights residues implicated in enzymatic activity towards mono-ADP-ribosylated ARTD10 (818-1025). (d) ADP-ribose binding (under high and low salt conditions) to WT and mutant MacroD2 (left) or MacroD1 (right) was assessed with His- and GST-tagged, recombinantly expressed macrodomain proteins that were immobilized on glutathione or Nickel sepharose and incubated with automodified ARTD10.

Supplementary Figure 4

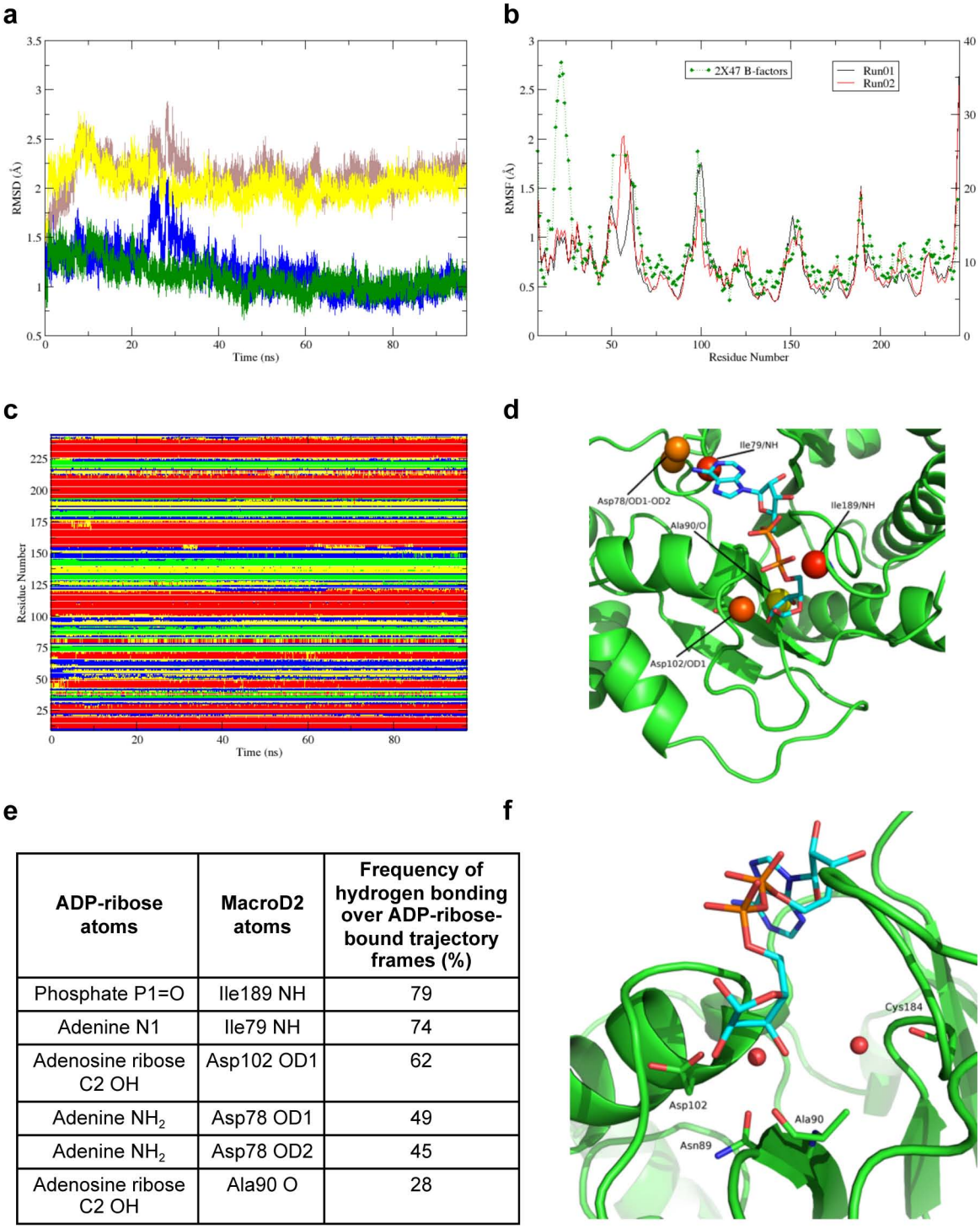

e

ADP-ribose atoms	MacroD2 atoms	Frequency of hydrogen bonding over ADP-ribose-bound trajectory frames (%)
Phosphate P1=O	Ile189 NH	79
Adenine N1	Ile79 NH	74
Adenosine ribose C2 OH	Asp102 OD1	62
Adenine NH_2	Asp78 OD1	49
Adenine NH_2	Asp78 OD2	45
Adenosine ribose C2 OH	Ala90 O	28

Supplementary Figure 4. Validation of the MacroD2 homology model and docking and molecular dynamics simulations of ADP-ribose in MacroD2. (a) Time evolution of Cα atoms Root Mean Square Deviation (RMSD) from the MacroD2 homology model. Yellow and brown lines: Cα atoms of residues having an RMSF value of less than 1 Å (shown in panel B) for independent molecular dynamics runs I and II, respectively. Green and blue lines: Cα atoms of the putative binding site for independent molecular dynamics runs I and II, respectively. (b) Cα atom Root Mean Square Fluctuations (RMSF) along the sequence of MacroD2 for molecular dynamics runs I (black) and II (red). B-Factors of template Human MacroD1 (PDB ID: 2X47) are shown in green. (c) Time evolution of secondary structure [1,2] of MacroD2 for molecular dynamics run I. Red: α-helix. Green: β-sheet or β-bridge. Yellow: bend or helix-turn. Blue: loop. The secondary structure evolution was likewise stable for run II. (d) MacroD2 atoms participating in among frames in which ADP-ribose was in the binding site. Atoms are coloured on a red (high)-yellow (low) scale according to frequency of hydrogen bond occurrence. (e) Quantification of frequency of hydrogen-bonding of ADP-ribose to residues of MacroD2. (f) Water molecules close to ADP-ribose forming stable hydrogen-bonding interactions with residues of MacroD2.

Supplementary note:

Homology modeling of MacroD2

Modeling of the three-dimensional structure of residues 9 to 244 of the human MacroD2 protein was undertaken using Modeller (version 9.10) [3-6]. As template, the coordinates of residues 90 to 325 of apo human MacroD1 (PDB ID: 2X47) were selected following alignment of the FASTA sequences of these residues (UniProt ID: Q9BQ69) and residues 9 to 244 of human MacroD2 (UniProt ID: A1Z1Q3) using CLUSTAL O version 1.1.0 on UniProt [7], giving an identity of 53.6%.

The MacroD2 homology model having the lowest Discrete Optimized Protein Energy assessment score [8] was subject to steepest-descent minimisation and explicit-water molecular dynamics (MD) simulations using GROMACS [9] (version 4.5.4) with the CHARMM22 force field [10] and TIP3P water model [11]. Aspartate and glutamate side-chains were negatively charged and those of lysines and arginines were positively charged, while histidines were maintained as neutral. The N-terminus of the protein was acetylated and the C-terminus N-methyl amidated. The protein was immersed in an orthorhombic box of pre-equilibrated water molecules having a minimal distance of 12 Å between the boundary and any protein atom. Sodium and chloride ions were added to the systems for an ion concentration of 150 mM.

The van der Waals and short-range electrostatic interactions were determined up to a cutoff of 10 Å. Periodic boundary conditions were applied and long-range electrostatic interactions were evaluated using the particle-mesh Ewald summation method [12]. MD simulations were performed in the NPT-ensemble at constant temperature (310 K) using the modified Berendsen thermostat, and constant pressure (1 atm) using the Parrinello-Rahman barostat [13]. Covalent bonds involving hydrogen atoms were constrained using the Linear Constraint Solver algorithm [14] and the time-step was 2 fs.

References

1 Andersen, C. A., Palmer, A. G., Brunak, S. & Rost, B. Continuum secondary structure captures protein flexibility. *Structure* **10**, 175-184, (2002).

2 Carter, P., Andersen, C. A. & Rost, B. DSSPcont: Continuous secondary structure assignments for proteins. *Nucleic Acids Res* **31**, 3293-3295, (2003).

3 Eswar, N. *et al.* Comparative protein structure modeling using Modeller. *Current Protoc Bioinformatics* **Chapter 5**, Unit 5 6, (2006).

4 Marti-Renom, M. A. *et al.* Comparative protein structure modeling of genes and genomes. *Annu Rev Biophys Biomol Struct* **29**, 291-325, (2000).

5 Sali, A. & Blundell, T. L. Comparative protein modelling by satisfaction of spatial restraints. *J Mol Biol* **234**, 779-815, (1993).

6 Fiser, A., Do, R. K. & Sali, A. Modeling of loops in protein structures. *Protein Sci* **9**, 1753-1773, (2000).

7 Reorganizing the protein space at the Universal Protein Resource (UniProt). *Nucleic Acids Res* **40**, D71-75, (2012).

8 Shen, M. Y. & Sali, A. Statistical potential for assessment and prediction of protein structures. *Protein Sci* **15**, 2507-2524, (2006).

9 Hess, B., Kutzner, C., van der Spoel, D. & E., L. GROMACS 4: Algorithms for Highly Efficient, Load-Balanced, and Scalable Molecular Simulation. *J Chem Theory Comput.* **4**, 435-447, (2008).

10 MacKerell, A. D. *et al.* All-Atom Empirical Potential for Molecular Modeling and Dynamics Studies of Proteins†. *J Physical Chem B* **102**, 3586-3616, (1998).

11 Jorgensen, W. L., Chandrasekhar, J., Madura, J. D., Impey, R. W. & Klein, M. L. Comparison of simple potential functions for simulating liquid water. *J Chem Phys* **79**, 926-935, (1983).

12 Essmann, U. *et al.* A smooth particle mesh Ewald method. *J Chem Phys* **103**, 8577, (1995).

13 Parrinello, M. & Rahman, A. Polymorphic transitions in single crystals: A new molecular dynamics method. *J Appl Phys* **52**, 7182, (1981).

14 Hess, B., Bekker, H., Berendsen, H. J. C. & Fraaije, J. G. E. M. LINCS: A linear constraint solver for molecular simulations. *J Comput Chem.* **18**, 1463-1472, (1997).